Lawrence Berkeley Laboratory
UNIVERSITY OF CALIFORNIA

Materials & Molecular Research Division

Presented at the TMS-AIME Symposium on "Nondestructive Evaluation - Microstructural Characterization and Reliability Prediction", Pittsburgh, PA, October 4-8, 1980; and to be published in the Proceedings

NON-DESTRUCTIVE FAILURE PREDICTION FOR BRITTLE SOLIDS

A.G. Evans

October 1980

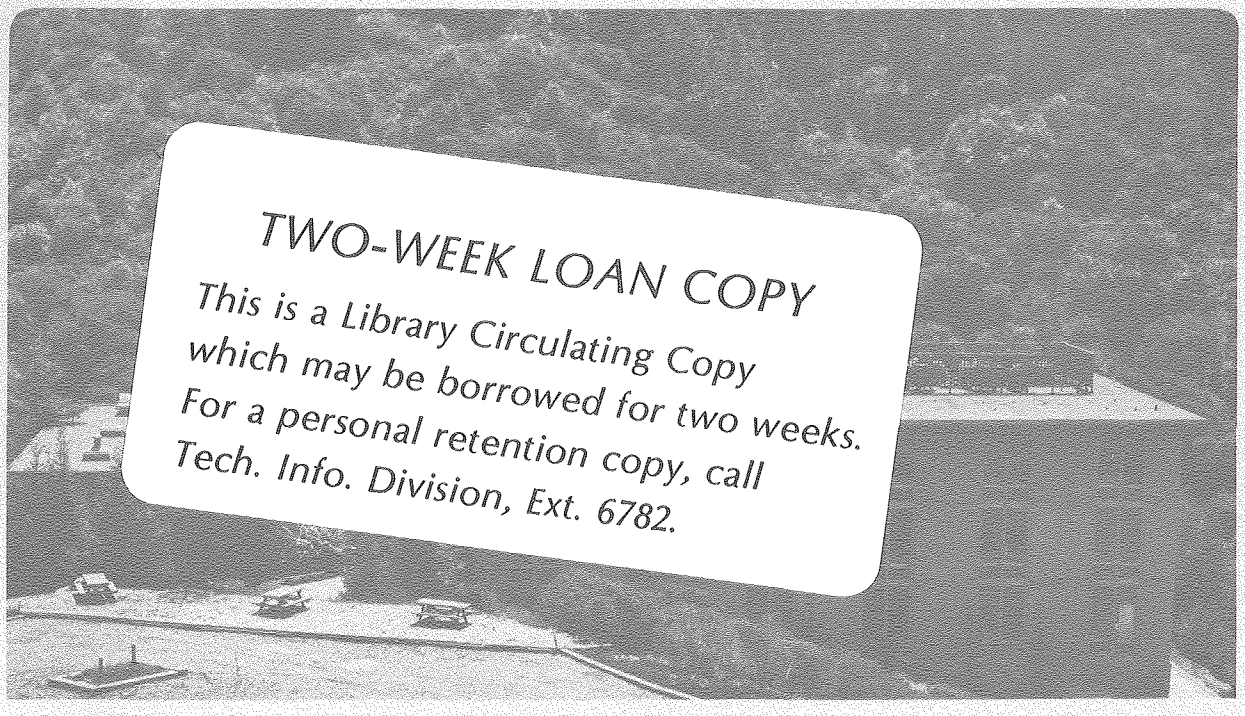

Prepared for the U.S. Department of Energy under Contract W-7405-ENG-48

DISCLAIMER

NON-DESTRUCTIVE FAILURE PREDICTION FOR BRITTLE SOLIDS

A.G. Evans

Lawrence Berkeley Laboratory
Materials Science and Mineral Engineering
University of California, Berkeley, CA 94720

ABSTRACT

Structural design with brittle materials requires that the stress level in the component correspond to a material survival probability that exceeds the minimum survival probability permitted in that application. This can be achieved by developing failure models that fully account for the probability of fracture from defects within the material (including considerations of fracture statistics, fracture mechanics and stress analysis), coupled with non-destructive techniques that determine the size of the large extreme of critical defects. Approaches for obtaining the requisite information are described in this paper.

1. Introduction

The design of structural components from brittle solids is, in concept, quite straightforward. It simply requires that the stress level in the component should not exceed the strength of the material, at the permissible level of survival probability. The implementation of this concept is, however, rather involved. It requires the combination of information derived from the disciplines of fracture statistics, fracture mechanics and flaw detection (or non-destructive evaluation). The description of the general scientific framework for structural design, utilizing these disciplines, is the primary intent of the present paper.

Ultimately, design might take the form of a computer simulation of crack growth in real microstructures, coupled with microstructural characterization techniques (such as acoustic scattering). Presently, however, useful progress is being achieved using a partially decoupled approach. The evolution of failure from defects and the crack extension mechanisms are studied separately, and merged where possible. This approach has influenced the structure of the paper, which includes separate considerations of fracture initiating flaws and defect characterization.

The character of the design problem is illustrated in Fig. 1a, which plots the probability of fracture of a ceramic (measured, say, in flexure) as a function of stress level. It might be construed that for design purposes, it is simply necessary to superimpose the permissible level of failure onto this figure, to obtain a maximum allowable stress in the component: and then to design the component accordingly. The limitations of this approach are exposed when it is appreciated that the fracture probability curve can be substantially perturbed by a wide variety of phenomena. These include: the incidence of slow crack growth (Fig. 1b), the occurrence of undetected flaw populations in the inevitable region of extrapolation (Fig. 1c), and effects of stress state (Fig. 1d). Because of the problems associated with the direct use of statistical design procedures, alternate approaches have been sought, which attempt to effectively truncate the strength distribution at a level above the design stress (Fig. 1e). One such approach, involving the characterization of fracture initiating defects and of the evolution of failure, is emphasized in the present paper.

Fracture in brittle solids usually occurs either by the direct extension of a single pre-existent flaw (from the large extreme of the flaw population) or by the coalescence of small flaws. The level of stress needed to activate these flaws relates to the size of the flaw in a manner that depends upon the interaction of the flaw with the surrounding microstructure. The

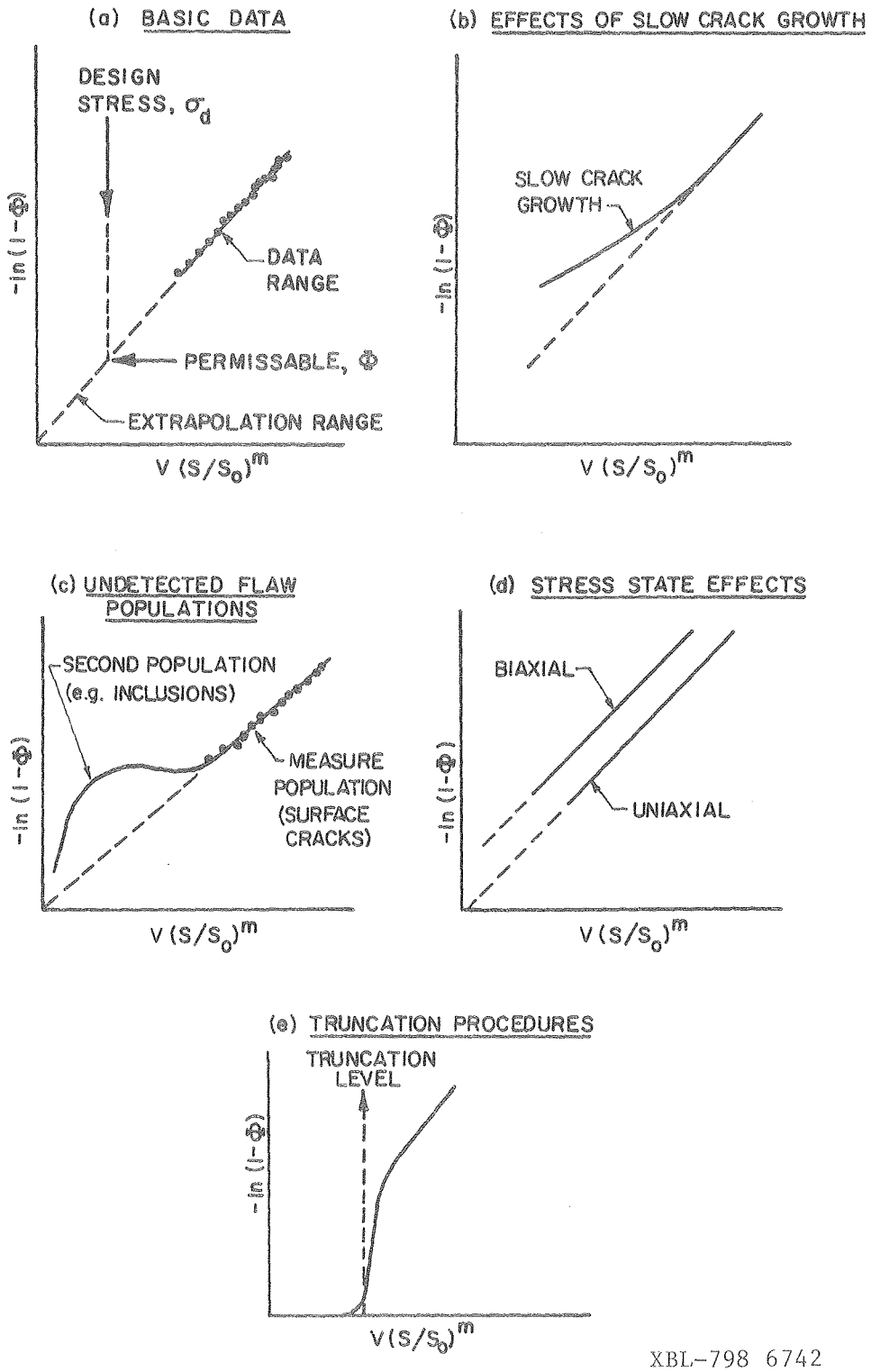

Fig. 1. A schematic illustrating some of the issues that limit the use of a direct statistical approach for structural design. The diagrams relate the fracture probability Φ to the strength level S and the sample volume V.

character of these interactions and the resultant strength, flaw size, probability relations are described in the first part of the paper, for each of the prevalent flaw types: inclusions, voids, surface cracks, microcracks.

The ultimate survival of a brittle structural component at an acceptable survival probability requires the use of a flaw characterization technique in conjunction with a failure model. Such techniques involve the detection and analysis of waves scattered or absorbed by defects. The most versatile and sophisticated mode of flaw characterization involves the use of acoustic waves: either bulk waves of surface waves. The utility of acoustic waves for providing the requisite survival information, including the combination of the measurement and fracture results to derive optimum accept/reject decision schemes, is described in the second part of the paper.

2. Fracture Initiating Defects

The flaws that ultimately initiate fracture in brittle solids can be conveniently classified as intrinsic or extrinsic. The intrinsic flaws are introduced during the fabrication and are predominantly inclusions or voids. The extrinsic flaws are stress induced cracks, such as the surface cracks introduced during machining and the microcracks that result from large residual stresses (e.g., due to thermal contraction anisotropy). Each class of defect will be discussed separately.

The only available analyses of fracture from defects that provide a consistent description of effects of defect size, type and shape invoke the existence of preexistent microflaws, activated by the concentrated stress fields around and within the defects. (1,2,3) However, the character of these small flaws is not well-defined. It is supposed that the flaws are the small voids (or precipitates) that typically occur at grain boundaries (e.g., at triple points). These flaws are prone to activation at relatively small levels of applied stress because of the large residual stresses that can exist at grain boundaries due to thermal contraction anisotropy (4) (Fig. 2); such flaws located on high energy boundaries would be particularly susceptible to microcrack formation. Direct evidence of this mode of microcracking has not been obtained, however, and the concept must be treated as phenomenological at this juncture.

The statistical character of the microcracking process can be conveniently posed by commencing with the premise that the microflaws exhibit an extreme value size distribution that leads to the probabilistic relation (5,6);

$$\Phi(a) = 1 - \exp[-(A/A_o)(a_o/a)^k] \qquad (1)$$

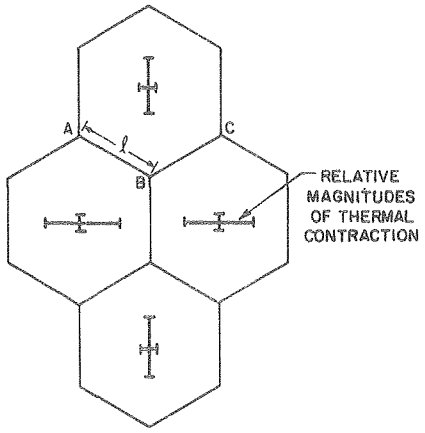

(a) FOUR GRAIN ARRAY

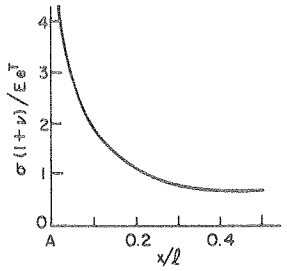

(b) STRESS ALONG FACET AB

XBL-796 6913

Fig. 2. Stresses caused by thermal expansion anisotropy.

where $\Phi(a)$ is the probability of finding a microflaw larger than $\underline{a}$ on a grain boundary of area A, a_o is a scale parameter, k is a shape parameter and A_o is a normalizing constant. Noting that a flaw will extend under the condition that the stress intensity factor K reaches the critical value for grain boundary fracture, $K^c_{g.b}$, then gives the approximate result (7,8);

$$\frac{\pi\left(K^c_{g.b}\right)^2}{4a} \approx \sigma^2 + \frac{4\tau^2}{(2-\nu)^2} \tag{2}$$

where σ is the total stress (applied plus residual) normal to the boundary and τ is the total in-plane shear stress needed to induce crack extension. Substituting $\underline{a}$ from Eq. (2) into Eq. (1) gives the probability of microcracking as a function of applied stress $(\sigma_\infty, \tau_\infty)$ as:

$$\Phi(\sigma_\infty, \tau_\infty) = 1-\exp\left[-\left(\frac{1}{A_o}\right)\left(\frac{4a_o}{\pi}\right)^k \int_A \left(\frac{(2-\nu)^2(\sigma_\infty+\sigma_R)^2+4(\tau_\infty+\tau_R)^2}{K^c_{g.b}(2-\nu)^2}\right)^k dA\right]. \tag{3}$$

It should be noted that, since the residual stresses and the toughness are variables, the microcrack probability associated with a specific boundary is not uniquely related to the applied stress; rather, a distribution of probabilities generally exists. However, for many problems, the probability of crack formation averaged over many grains is most pertinent. The average residual stress must then be zero, and Eq. (3) reduces to the simple form;

$$\Phi(\sigma_A) = 1 - \exp\left[-\frac{1}{V_o}\int_V (\sigma_A/S_o)^m \, dV\right] \tag{4}$$

where σ_A is the applied stress, m is the shape parameter (=2k), S_o is the scale parameter (which includes $K^c_{g.b}$, a_o and ν as well as a coefficient that reflects an averaging of the normal and shear stresses over the grain boundaries) and V is the volume of material. A relation similar to Eq. (4) is also generally assumed to describe microcrack extension, except that S_o will have a different significance.

2.1 Intrinsic Defects

(a) Voids. The probability of fracture from a void can be ascertained by combining the void stress field with the appropriate statistical relation for extension of microcracks existing in the vicinity of the void. If the microcracks are very much smaller than the void radius, a direct statistical analysis using Eq. (4) suffices. (1,2) For example, when the microcracks predominate at the void surface (Fig. 3), the surface stress field (9);

$$\begin{aligned} \sigma_\theta/\sigma_A &= [3/2(7-5\nu)]\,[(4-5\nu) + 5\cos 2\theta] \\ \sigma_\alpha/\sigma_A &= [3/2(7-5\nu)]\,[5\nu\cos 2\theta - 1] \end{aligned} \tag{5}$$

can be combined with Eq. (4), and integrated over the tensile portion of the void surface, to yield (2);

$$\xi \equiv -\ln[1-\Phi] \approx 8r^2(\sigma_A/S_o)^m \exp[0.52m - 1.4] \tag{6}$$

where r is the void radius. A stronger dependence on r emerges for volume distributed microflaws, viz., $\xi \propto r^3$, as deduced by Vardar, et al. (1)

When the microcracks are not small, vis-a-vis the void radius, a stress gradient correction derived from fracture mechanics solutions must be applied. (2) This correction arises because the stress intensity factor for

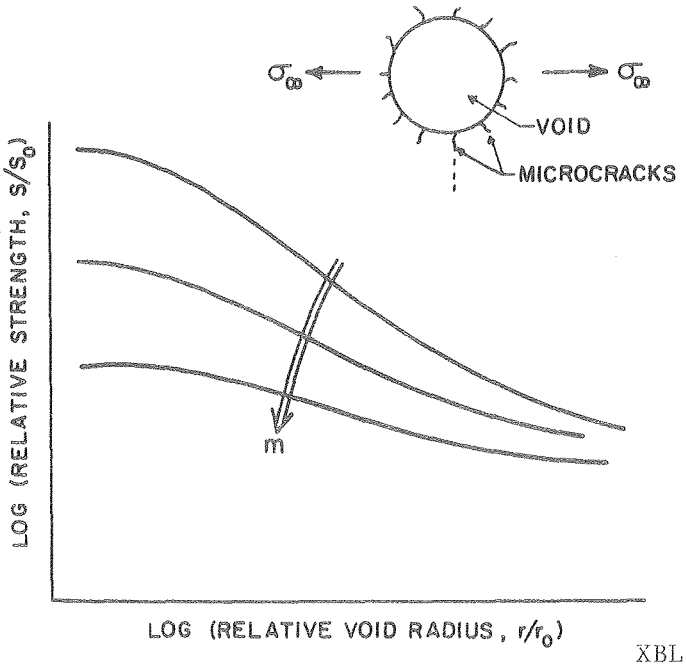

XBL 798-6910

Fig. 3. A schematic illustrating flaws distributed at the void surface, and the fracture strength, void size relation derived at constant probability.

a flaw located in a rapidly varying stress field depends sensitivity on the exact flaw location and on its size relative to the gradient. The effect is especially manifest for surface located microcracks, which are subject to the following approximate peak stress intensity factor (2);

$$\hat{K} = \frac{2\sigma_A \sqrt{a}}{\sqrt{\pi}\,[1+0.3\ (0.2+a/r)]} \,. \tag{7}$$

This relation for $\hat{K}$ can be used to obtain an effective stress σ_{eff}, that replaces the applied stress in Eq. (16), given by;

$$\sigma_{eff} = \sigma_A \left\{ 0.3+0.7[1+\alpha/2)^2]^{-1} \right\}$$

where $\alpha = (1/r)(K_c/\sigma_A)^2$. Typical void size, strength relations at constant probability, predicted by this analysis, are plotted in Fig. 3.

The basic pertinence of the statistical approach for describing strength in the presence of voids, has been substantiated for voids in silicon nitride (3) and in PZT (1). A detailed statistical analysis was conducted for the experiments performed on silicon nitride. This analysis revealed a maximum likelihood estimate of the void radius dependence of 2.1 and demonstrated

that the coefficients m and S_o were independent of the void radius, with maximum likelihood estimates of $\hat{m} = 4.6$ and $\hat{S}_o = 106$ MPa.

(b) Inclusions. Several modes of failure have been associated with the presence of inclusions. The first distinguishing feature is the tendency for cracking due to thermal contraction mismatch (10,11) (Fig. 4). If the thermal expansion coefficient of the inclusion is appreciably lower than that for the matrix, radial matrix cracks can initiate when the defect exceeds a critical size. This situation can produce severe strength degradation. This is, however, an unusual condition for structural brittle materials, which must have an intrinsically low thermal expansion coefficient in order to resist thermal shock. Alternately, if the expansion coefficient

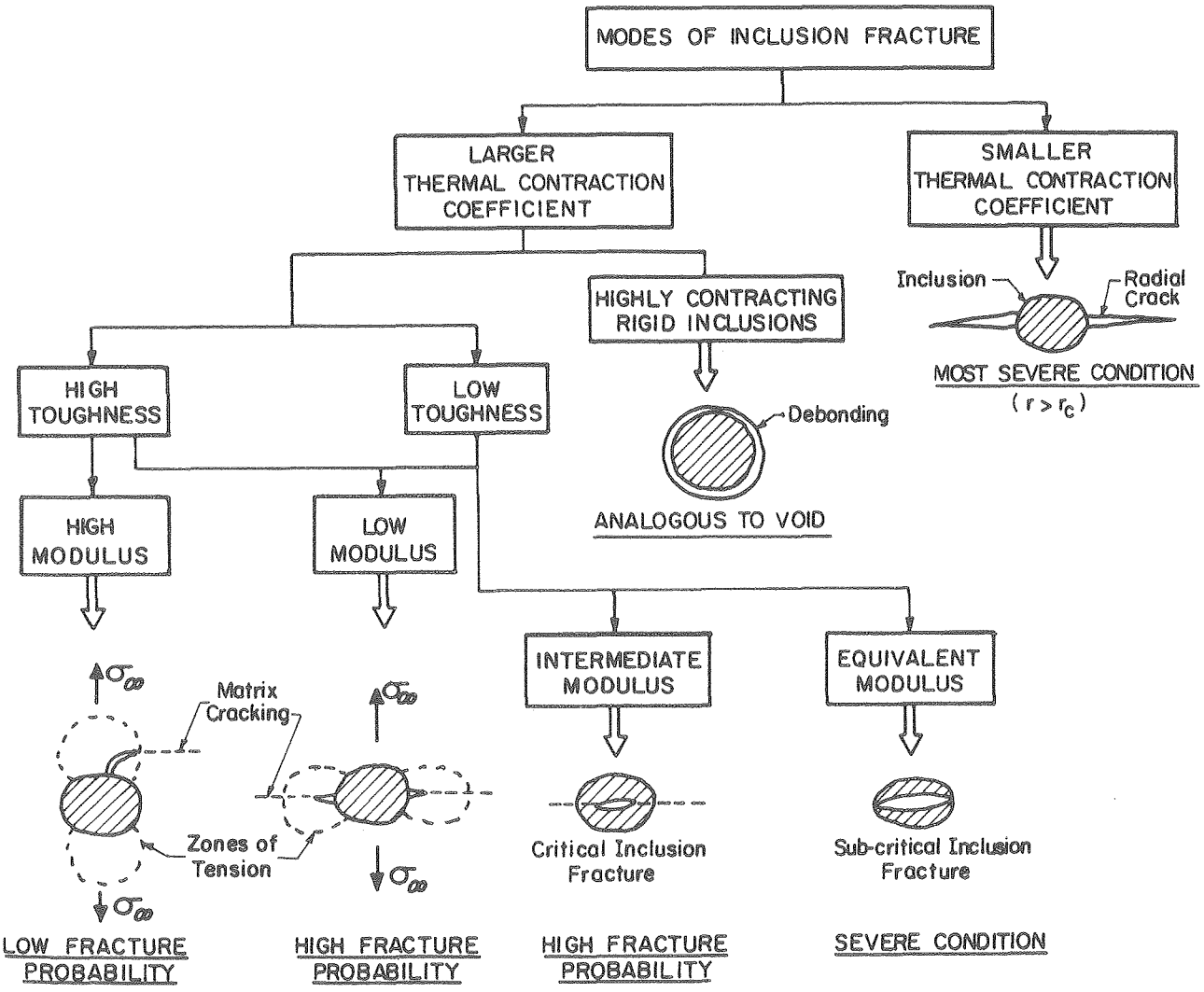

XBL 798-6740

Fig. 4. A schematic indicating the various cracking responses that can occur in the presence of inclusions.

of the inclusion exceeds that of the matrix, several possibilities can result. Highly contracting, high modulus inclusions will tend to detach from the matrix, tending to produce a defect comparable in character to a void. Inclusions that are more compliant or exhibit smaller relative contractions, remain attached to the matrix. Thereupon, several modes of failure are possible, as exemplified by the results for several types of inclusion in silicon nitride (3) (Fig. 5). The expected failure mode depends upon the elastic modulus and fracture toughness of the inclusion, vis-a-vis the matrix. When the inclusion has a larger toughness than the matrix (an unusual occurrence) fracture initiates within the matrix, usually from microflaws located within (or adjacent to) the interface. The process then resembles the void fracture problem. However, one additional distinction must be introduced. When the bulk modulus of the inclusion exceeds that of the matrix, the tensile stresses (in a direction suitable for continued extension of the crack due to the applied stress) are confined to a relatively small zone near the poles of the inclusion (Fig. 4). The fracture probability can then be anticipated to be relatively small, as exemplified by the high survival probability for WC inclusions in silicon nitride. Alternatively, when the modulus of the inclusion is smaller than that for the matrix, the maximum tensile stresses occur near the equatorial plane. The fracture condition is then comparable to that for a void, modified by a stress coefficient λ that depends on the modulus ratio;

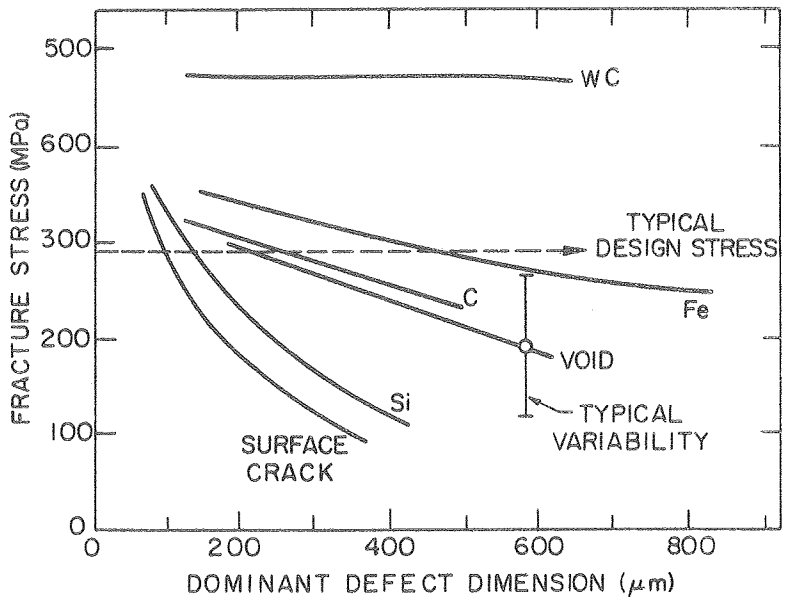

XBL-796 6419

Fig. 5. Strength, size relations for various fracture initiating defects in silicon nitride.

$$\lambda = 1 + \frac{2[(\kappa_i/\kappa_m) - 1](1-2\nu)}{3(1-\nu)} \left[\frac{4\mu_m + 3\kappa_m}{4\mu_m + 3\kappa_i}\right] \tag{9}$$

where κ is the bulk modulus and μ is the shear modulus. This case is expected to be an important one in ceramics, because the inclusions are often porous (3) (following high temperature mass transport driven by thermal contraction anisotropy) and hence, of low effective modulus.

Most inclusions typically encountered in brittle matrices are of low toughness, because they are usually the friable product of chemical reaction with the matrix (12) (Fig. 6). If such an inclusion also has a relatively high modulus (approaching that of the matrix), the inclusion can fracture sub-critically to create a crack of dimensions comparable to the cross-section of the inclusion. The ultimate fracture strength is then dictated by the usual fracture mechanics relation for an internal crack (13)

$$\sigma = z(a/c) K_c^M a^{\beta} F(\kappa_m/\kappa_i) \tag{10}$$

where a and c are the dimensions of the crack, K_c^M is the effective toughness of the matrix phase neighboring the defect and β is an exponent (≈ 0.5) that depends on the modulus ratio. This type of defect is the most deleterious

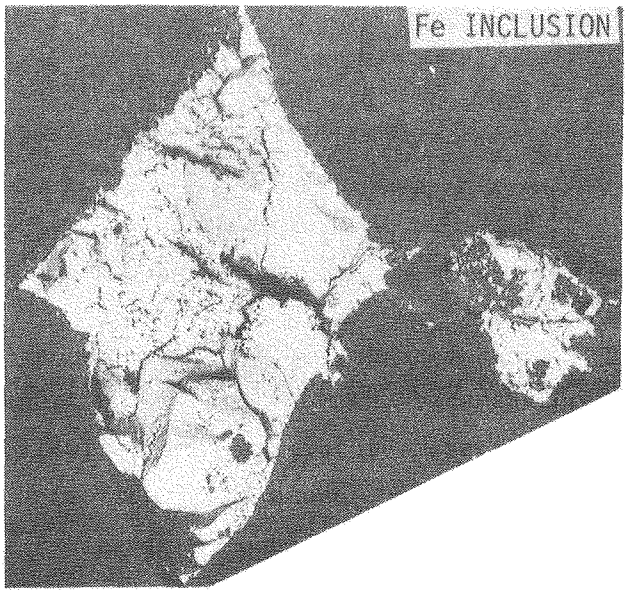

XBB 796-8388

Fig. 6. A scanning electron micrograph of an iron silicide inclusion in silicon nitride.

of the high expansion defects (Fig. 4). Defects in this category are exemplified by Si inclusions in Si_3N_4 (Fig. 5). When the modulus of the defect becomes very small, because of extensive porosity (Fig. 6), the stresses do not attain a sufficient level to induce defect fracture (despite their friability); the situation is then identical to that of low modulus, high toughness inclusions. However, an intermediate condition is also possible; wherein fracture can initiate within the defect and then propagate directly into the matrix to cause complete failure. In this situation, fracture is dictated by the probability of activating microflaws within the inclusion, and the fracture probability becomes (3);

$$\Phi = 1 - \exp\left[-V_i \left(\frac{\lambda\sigma_\infty + \sigma_\alpha}{\rho_o} \right)^\gamma \right] \tag{11}$$

where ρ_o is the scale parameter, γ is the shape parameter, and V_i is the inclusion volume. Fracture results obtained for iron silicide inclusions in silicon nitride satisfy a joint fracture relation involving a combination of the critical defect fracture model (Eq. 11) and the matrix fracture model pertinent to low modulus inclusions. (3) This is a plausible situation considering the potential for a transition, with decrease in size, from inclusion initiated fracture (volume dependent) to matrix fracture (area dependent).

2.2 Extrinsic Defects

Extrinsic defects are usually cracks produced by large transient or localized stress states. The most common sources of extrinsic defects are surface cracks produced by machining (14), impact (15) or thermal shock. The machining induced cracks are the most prevalent (and comparable in character to the cracks introduced by projectile impact). (15) The evolution of the cracks, and their resultant influence on strength, is analogous to the cracking that occurs during indentation (16) (Fig. 7). The ultimate dimensions of the cracks are dictated by the residual indentation field, as controlled by the hardness, H, toughness, K_c, and modulus, E, of the material. A specific relation recently derived for the strength controlling radial cracks is (16);

$$a^{3/2} = 2.10^{-2} (\cot^{2/3}\psi)(E/H)^{2/3} K_c^{-1} P_N \tag{12}$$

where ψ is the included angle of the grinding particle and P_N is the normal

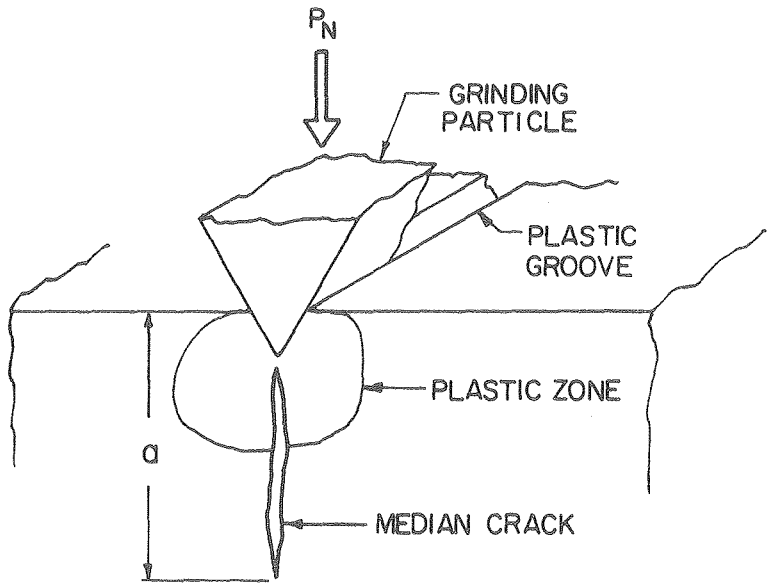

XBL 798-6743

Fig. 7. The median cracking that accompanies the grinding of ceramic surfaces.

force applied to the particle. The term E/H arises because fracture is a residual stress dominated process. (17) The radial cracks are usually semi-circular, because of the symmetry of the residual field.

The extension of the surface cracks introduced by grinding is explicable using standard fracture mechanics relations for mode I[13],

$$K = F(\theta) \frac{2}{\sqrt{\pi}} \sigma \sqrt{a} \tag{13}$$

where $F(\theta)$ is a function that describes the variation in K_I around the crack periphery. Extension to the mixed mode fracture of inclined cracks appears to be adequately described, over an appreciable angular range, by the simple coplanar strain energy release rate criterion. (18) However, the effective stress that produces crack extension can include a significant residual component particularly in coarse grinding situations, where the plastic zone is not removed by subsequent fine grinding. Consequently, the applied stress at fracture can exhibit both systematic and random variations from that anticipated by direct application of Eq. (13) (with the peak stress intensity factor $\hat{K}$ equated to K_c). Available test results suggest a probability of fracture given by the normal distribution (19)

$$\Phi(\sigma_\infty | \sigma_\rho) = \frac{1}{v\sqrt{2\pi}} \int_{-\infty}^{\sigma_\infty} \exp\left[\frac{\sigma_\infty - a + \beta\sigma_\rho}{\sqrt{2}\, v}\right]^2 d\sigma_\infty \tag{14}$$

where σ_ρ is the predicted strength obtained from Eq. (13);

$$\sigma_\rho = \frac{K_c}{\hat{F}(\theta)} \quad \frac{\sqrt{\pi}}{2\sqrt{a}} \tag{15}$$

$\hat{F}(\theta)$ corresponds to the value at $\hat{K}$, v is the variance in σ_ρ, β is a systematic error coefficient and α is a parameter related to the mean strength.

3. Non-Destructive Defect Characterization

3.1 Accept/Reject Criteria

Accept/reject decisions based on a non-destructive measurements of scattering from a defect must recognize the probabilistic character of the problem. (20) At least three probabilities enter the analysis: the failure probability, given the defect dimensions (discussed above) $\phi(\sigma_\infty^c|a)d\sigma$; the joint probability of identifying the defect type and of estimating its size, $\phi(a_{es}|a)da_{es}$; the a priori distribution of defect size, $\phi(a)da$. These probabilities are combined and integrated to various inspection levels, a_{es}^*, to obtain two interrelated probabilities: the false-accept probability Φ_A and the false-reject probability, Φ_R (Fig. 8a):

$$\Phi_A = \int_0^{\sigma_A} \int_0^{a_{es}^*} \int_0^{\infty} \left[\phi(\sigma_\infty|a)d\sigma_\infty\right]\left[\phi(a_{es}|a)da_{es}\right]\left[\phi(a)da\right] \tag{32}$$

$$\Phi_\Theta = \int_{\sigma_A}^{\infty} \int_{a_{es}^*}^{\infty} \int_0^{\infty} \left[\phi(\sigma_\infty^c|a)d\sigma_\infty\right]\left[\phi(a_{es}|a)da_{es}\right]\left[\phi(a)da\right]$$

where σ_A is the level of the applied tension in the volume element containing the defect. The inspection level a_{es}^* refers to the estimated defect dimension(s) selected for the rejection or acceptance of the component, e.g., all components with an estimated maximum dimension less than a_{es}^* are accepted and all components with an estimated dimension greater than a_{es}^* are rejected. The false-accept probability Φ_A is thus the probability that components accepted in accord with the specified inspection level will contain defects more severe than indicated by the estimate, and will actually fail in service (i.e., related to the failure probability). This probability decreases, of course, as the inspection level decreases (Fig. 8b). The false-reject probability Φ_R is the (related) probability that rejected components would, in fact, have performed satisfactorily in service, because the defect severity has been overestimated by the selected inspection level.

This probability increases as a^*_{es} decreases (Fig. 8b). However, it is crucial to recognize that these probabilities are interrelated, i.e., they merely represent different ranges of integration of the same combination of probability functions (Eq. 16). This interdependence is exemplified in Fig. 8a, which is a typical plot relating the false-accept and false-reject probabilities. Once one of these probabilities has been selected, the other probability, as well as the associated inspection level, are necessarily defined. It is now apparent from Fig. 8b that the inspection technique, or combination of techniques, that would be preferred is that which yields a curve as close as possible to the probability axes. For example, technique B is preferred over technique A, because the rejection of satisfactory components required to satisfy the failure probability requirements is much lower. Such curves thus represent a quantitative method for characterizing the failure prediction capabilities of various inspection techniques, for a given material and service condition.

Scrutiny of the available inspection methods pertinent to ceramics indicates that acoustic methods are preferred, because acoustic waves are appreciably scattered by all of the critical defect types encountered in structural ceramics. The most promising measurement algorithms and their future potential are thus briefly reviewed.

3.2 Acoustic Measurement Algorithms

Surface Waves. The most directly applicable acoustic method is the use of surface acoustic waves to predict failure from surface cracks: in particular, the use of long wavelength, $\lambda \gg a$, surface waves. (21,22) In the long wave length limit, the scattering of an acoustic wave (stress wave) by a crack is closely analogous to the interaction of the crack with an applied stress field. In particular, both the scattering coefficient S_1 and the strain energy release rate $\mathcal{G}$ are related to the crack surface integral (21);

$$\int_{A_s} \sigma_{ij} \Delta u'_j n_i dA_s$$

where σ_{ij} is the stress across the crack plane in the absence of the crack, $\Delta u'_j$ is the displacement of the crack surfaces and A_s is the crack surface area. Hence, it is straightforward to demonstrate that the scattering coefficient when the acoustic beam is aligned with the tensile axis in the compound is directly related to the crack extension stress σ_c by (22);

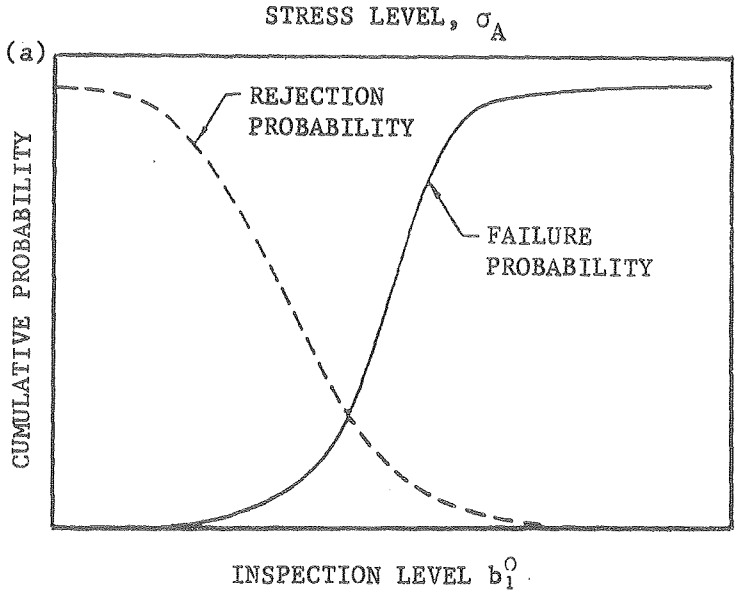

Fig. 8a. False-accept, false-reject curves for two hypothetical measurement techniques, A and B.

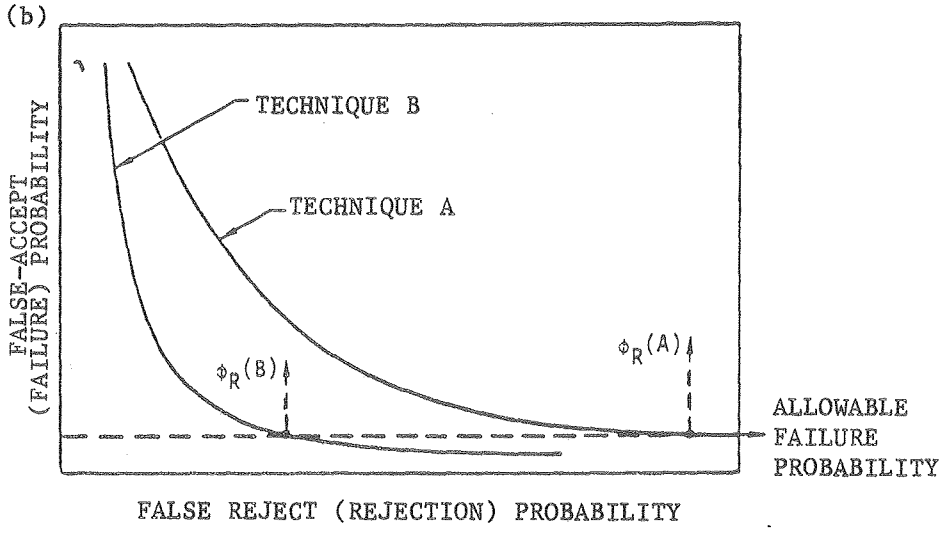

Fig. 8b. The variations of failure probability and rejection probability with inspection level.

XBL 797-10502

$$\frac{K_c}{\sigma_c} = 2\left[\frac{6(1-\nu)\lambda^2 S_i w}{\pi^5 f_z \nu}\right]^{1/6} \tag{33}$$

where w is the beam width, η is the transducer efficienty and $f_z \sim 0.4$. This result is strictly correct when both the acoustic wave and the applied stress are normal to the crack plane, as exemplified by recent results for glass (22).

The prediction of failure based on surface acoustic wave measurements is more complex when the surface cracks are introduced by machining. (19) The crack formation occurs in response to a residual elastic/plastic field (16), that normally remains (at least in part) when the machining operation has been completed. (23) This residual field causes sub-critical crack extension when a remote tension is applied to the system. This crack extension is manifest in an irreversible change in the acoustic scattering coefficient as an external stress is applied (19). The crack length at fracture is thus appreciably larger than the initial length (by ~ 2.5) and hence, a failure estimate based on the initial length would provide a substantial underestimate of the failure stress.

The residual stresses can be largely removed by annealing at ~ 1200°C. The amplitude of the acoustic signal is thus only influenced by the load through the separation of contacting crack surfaces. The initial acoustic measurement after annealing thus relates more directly to the failure prediction.

Finally, it is noted that surface waves have the advantage that they propagate over curved surfaces, so that complex shapes can be readily probed. (22)

Bulk Waves. The characterization of bulk defects is more complex. Information over a wide range of frequencies appears to be needed to obtain a highly probable defect type classification and hence, a size estimation. Appropriate techniques are available including (24): the scanning laser acoustic microscope, 200 MHz ZnO transducers and conventional (2-50 MHz) transducers. Rapid scanning methods for defect location have also been developed. The most critical issue, therefore, concerns the appropriate choice of the algorithms to obtain the most reliable defect characterization. A typical set of algorithms and their interaction are illustrated in Table I, using low and high frequency information as well as acoustic microscopy. This set has not yet been fully evaluated, so redundancies may exist. Four algorighms are employed in this scheme: (i) long wave length scattering, (ii) intermediate wavelength Born approximation, (iii) high freuqency

Table 1

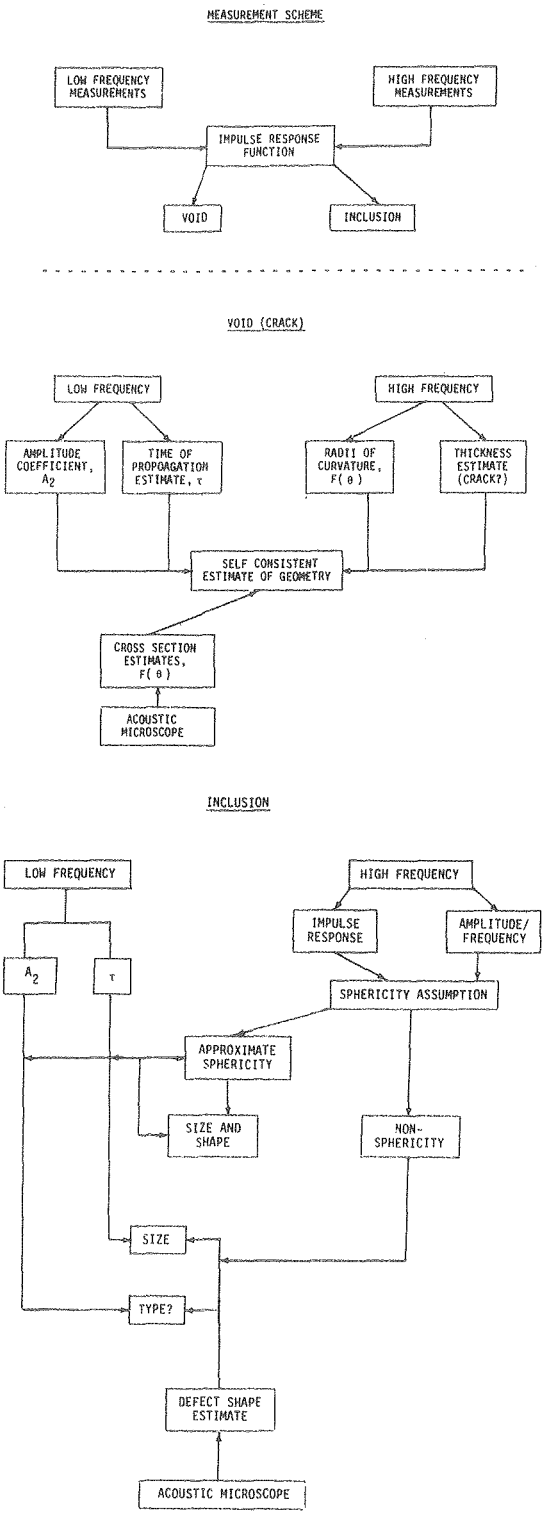

XBL 796 26328A

spectroscopy and (iv) cross sectional information from acoustic microscopy. The impulse response functions are firstly used to determine whether the defect is a void or an inclusion; the void has an impulse response function characteristic of the transducer, while inclusions have more complex functions. Thereafter, voids can be analyzed straightforwardly, using a variety of algorithms. For example, a long wavelength algorithm similar to that described for surface cracks may be employed. In the long wavelength limit the scattered amplitude is related to the void volume V by (20);

$$A = \frac{V\omega^2}{(4\pi c^2)2}\left[1 + \frac{1+\nu}{7-2\nu} + \frac{10(1-2\nu)}{7-5\nu}\right]^2 \qquad (34)$$

where ω is the frequency and c is the elastic wave speed in the host. Inclusions are more difficult to analyze; the combined use of several algorithms is almost certainly required. For nearly spherical inclusions, the interpretation is relatively straightforward. For example, a combination of the long wavelength algorithm (which contains coupled volume and type information) and the Born approximation (which provides an independent estimate of the distance from the geometric center to the back face of the inclusion) can yield the requisite size and type information. A typical result, obtained for a 100 μm radius Si inclusion in Si_3N_4, is illustrated in Fig. 9; wherein the joint probability of the defect type and size is plotted as a function of the estimated size. In order to obtain this result, six possible inclusion types were permitted to exist within the material (selected on the basis of detailed failure analyses conducted on this material). Alternatively, high frequency measurements displayed in the frequency domain would provide close estimates of the defect size and type.

3. Future Prospects

It is hoped that this paper conveys the impression that a positive start has been made in establishing the scientific framework for microstructural design with brittle materials. Certain rewarding research directions have emerged and several exciting near term, and more remove, prospects seem viable.

Further studies aimed at characterizing models of fracture from defects are very pertinent. The incisive combination of inputs from mechanics, materials and statistics demonstrated on the limited set of problems addressed thus far should provide some direction and scope for continued

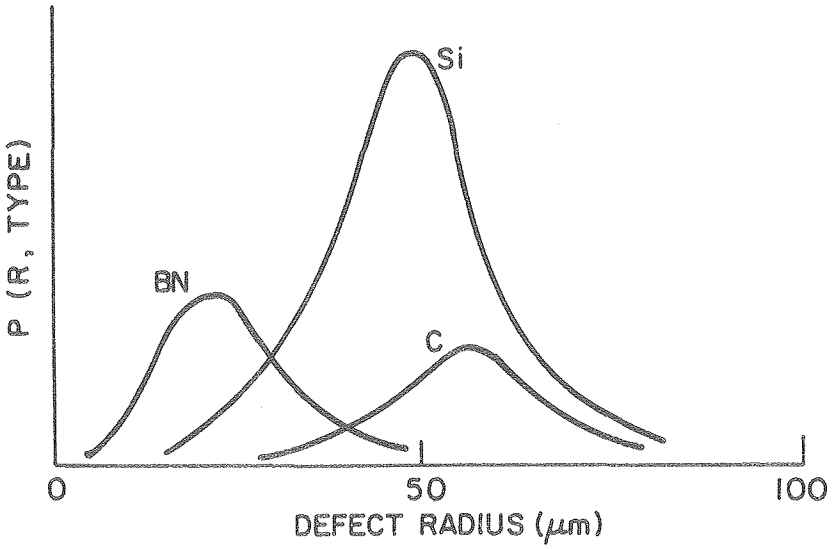

XBL 798-6912

Fig. 9. The joint probability of defect type and size deduced from a coupled long wavelength, Born approximation algorithm.

activity. Important defects not yet considered include: void clusters, sub-surface inclusions, surface crack arrays. Progress toward the comprehension of fracture from these defects could utilize existing (or marginally extended) stress analyses coupled with advanced statistical methods and fracture mechanics solutions.

Imminent advances can be anticipated in ultrasonic flaw characterization. A comprehensive set of inversion algorithms already exist, and initial results imply that good estimates of defect size and type are possible, using combinations of these algorithms. Future prospects for devising effective accept/reject schemes pertinent to ceramics are thus very exciting.

Acknowledgments

The author wishes to thank the Advanced Research Projects Agency for funding the work on fracture models and accept/reject criteria under Contract F 33615-74-5180, and the Office of Naval Research (A.G.E.) for supporting the work on surface crack detection, under Contract No. N0014-79-C-0159, and the U.S. Department of Energy under Contract W-7405-ENG-48.

References

1. O. Vardar, I. Finnie, D.R. Biswas and R.M. Fulrath, Int'l. Jnl. Frac., 13 (1977) 218.
2. A.G. Evans, D.R. Biswas and R.M. Fulrath, Jnl. Amer. Ceram. Soc., 62 (1979) 101.
3. A.G. Evans, G. Meyer, K. Fertig, B.I. Davis and H.R. Baumgartner, Jnl. of Non-Destructive Evaluation, (Nov. 1980) in press.
4. A.G. Evans, Acta Met., 26 (1978) 1845.
5. A.M. Freudenthal, Fracture (Ed. H. Liebowitz) Vol. 2, Academic Press, N.Y. (1969) p. 592.
6. A.G. Evans, B.R. Tittmann, L. Ahlberg, G.S. Kino and B.T. Khuri-Yakub, Jnl. Appl. Phys., 49 (1978) 2669.
7. S.B. Batdorf and H.L. Heinish, Jnl. Amer. Ceram. Soc., 61 (1978) 355.
8. A.G. Evans, Jnl. Amer. Ceram. Soc., 61 (1978) 302.
9. S. Timoshenko and J.M. Goodier, Theory of Elasticity, McGraw Hill, N.Y. (1951).
10. A.G. Evans, Jnl. Mater. Sci., 9 (1974) 1145.
11. R.W. Davidge and T.J. Green, Jnl. Mater. Sci., 3 (1968) 629.
12. H.R. Baumgartner and D. Richerson, Fracture Mechanics of Ceramics (Ed. R.C. Bradt, D.P.H. Hasselman and F.F. Lange) Vol. 1 (1974) p. 367.
13. G.C. Sih, Handbook of Stress Intensity Factors, Lehigh Univ. Press (1973).
14. M.V. Swain, Fracture Mechanics of Ceramics, ibid. Vol. 3 (1978) p. 257.
15. A.G. Evans, M.E. Gulden and M. Rosenblatt, Proc. Roy. Soc., A361 (1978) 343.
16. B.R. Lawn, A.G. Evans and D.B. Marshall, Jnl. Amer. Ceram. Soc., in 63 (1980) 574.
17. D.B. Marshall and B.R. Lawn, Jnl. Mater. Sci., in press.
18. J.J. Petrovic and M.G. Mendiratta, Jnl. Amer. Ceram. Soc., 59 (1976) 163.
19. J. Tien, B.T. Khuri-Yakub, G.S. Kino, D.B. Marshall and A.G. Evans, Jnl. Amer. Ceram. Soc. to be published.
20. J.M. Richardson and A.G. Evans, Jnl. of Non-Destructive Evaluation, 1 (1980) 368.
21. B. Budiansky and J.R. Rice, Jnl. Appl. Mech., 45 (1978) 2.
22. B.T. Khuri-Yakub, G.S. Kino and A.G. Evans, Jnl. Amer. Ceram. 63 (1980) 65.
23. D.B. Marshall, R.R. Lawn, and J. Mecholsky, Jnl. Amer. Ceram. Soc., 63 (1980) 358.
24. R.B. Thompson, this issue.